JOURNAL OF GEOPHYSICAL RESEARCH, VOL. 113, D11206, doi:10.1029/2007JD009367, 2008

Global distribution of solid and aqueous sulfate aerosols: Effect of the hysteresis of particle phase transitions

Jun Wang,[1,2] Andrew A. Hoffmann,[1] Rokjin J. Park,[1,3] Daniel J. Jacob,[1] and Scot T. Martin[1]

Received 9 September 2007; revised 14 February 2008; accepted 14 March 2008; published 10 June 2008.

[1] The partitioning between solid and aqueous phases of tropospheric sulfate-ammonium particles is simulated with a global 3-D chemical transport model (CTM). The simulation explicitly accounts for the hysteresis of particle phase transitions by transporting aqueous sulfate and three solid sulfate forms (namely, ammonium sulfate, letovicite, and ammonium bisulfate). Composition-dependent deliquescence relative humidities (DRH) and crystallization relative humidities (CRH) are based on recent laboratory data. We find that the solids mass fraction on a sulfate basis is 0.34, partitioned as 93% ammonium sulfate, 6% letovicite, and 1% ammonium bisulfate. The fraction increases with altitude from 0.10 to 0.30 in the boundary layer to 0.60–0.80 in the upper troposphere. The dominance of solids in the upper troposphere arises in part from high sulfate neutralization, reflecting in our simulation a low retention efficiency of NH_3 upon cloud freezing. High sulfate neutralization is consistent with the few available observations in the upper troposphere. High acidity with a dominant aqueous phase, however, can occur following volcanic eruptions. Seasonal variation of the solids mass fraction in both the lower and upper troposphere is modulated by emissions of NH_3 from the terrestrial biosphere and biomass burning as well as by emissions of dimethylsulfide from the ocean biosphere. The timescale of phase transitions, as driven by changes in relative humidity, varies from 10 to 50 h in the boundary layer to 150–400 h in the upper troposphere. Omission of the hysteresis effect in the CTM by assuming that particle phase follows the lower side of the hysteresis loop increases the solids mass fraction from 0.34 to 0.56. An upper side assumption decreases the fraction to 0.17. Lower and upper side assumptions better approximate particle phase for high and low altitudes, respectively. Fluctuations in the CRH, which can be induced by other constituents in sulfate particles such as minerals or organic molecules, strongly affect the solids mass fraction in the boundary layer but not at higher altitudes. Further studies are needed to determine the effects of large solids mass fraction on heterogeneous chemistry and cirrus cloud formation.

Citation: Wang, J., A. A. Hoffmann, R. J. Park, D. J. Jacob, and S. T. Martin (2008), Global distribution of solid and aqueous sulfate aerosols: Effect of the hysteresis of particle phase transitions, *J. Geophys. Res.*, *113*, D11206, doi:10.1029/2007JD009367.

1. Introduction

[2] Sulfate particles are the largest anthropogenic contributors to the atmospheric fine-mode aerosol [*Seinfeld and Pandis*, 1998]. They form from the oxidation of emitted SO_2, producing sulfuric acid that rapidly condenses as an H_2SO_4-H_2O solution. The resulting aqueous particles can be partly or totally neutralized by atmospheric ammonia, and in the process they may become solids depending on relative humidity (RH).

[3] Whether the particles are solid or aqueous has important implications for their environmental effects [*Martin*, 2000; *Haywood and Boucher*, 2000]. Solid particles are smaller and scatter solar radiation back to space less effectively [*Ramaswamy et al.*, 2001; *Martin et al.*, 2004; *Wang and Martin*, 2007]. Aqueous particles modify atmospheric chemistry through reactions such as N_2O_5 hydrolysis [*Jacob*, 2000; *Kane et al.*, 2001] and secondary organic aerosol production [*Lim et al.*, 2005]. Solid particles may serve as ice nuclei and influence cirrus cloud formation [*Martin*, 1998; *Shilling et al.*, 2006; *Abbatt et al.*, 2006]. Quantifying these effects requires a global 3-D chemical transport model (CTM) that includes an explicit consideration of particle phase.

[1] School of Engineering and Applied Sciences, Harvard University, Cambridge, Massachusetts, USA.
[2] Now at Department of Geosciences, University of Nebraska–Lincoln, Lincoln, Nebraska, USA.
[3] Now at School of Earth and Environmental Sciences, Seoul National University, Seoul, South Korea.

0148-0227/08/2007JD009367$09.00

[4] Determination of particle phase in global models is complicated by a hysteresis effect, creating bifurcations between the equilibrium and metastable branches of the particle hygroscopic growth curve [*Spann and Richardson*, 1985; *Tang and Munkelwitz*, 1994; *Biskos et al.*, 2006a]. The phase therefore depends on the RH history of the air parcel. For example, ammonium sulfate crystals deliquesce at 80% RH at 298 K [*Clegg et al.*, 1998]. However, the crystallization RH at which an aqueous ammonium sulfate particle loses its water and becomes solid is 35% [*Martin et al.*, 2003; *Biskos et al.*, 2006b]. In consequence, for RH values between 35 and 80%, ammonium sulfate particles may be either solid or aqueous depending on the RH history of the air parcel. Within the sulfate-ammonium system, which is defined by pure sulfuric acid at one pole and ammonium sulfate at the other, the availability of gaseous ammonia determines the degree of neutralization. Depending on the ammonium content, three solid phases may form: $(NH_4)_2SO_4$ (ammonium sulfate, AS), $(NH_4)_3H(SO_4)_2$ (letovicite, LET), and NH_4HSO_4 (ammonium bisulfate, AHS). Sulfuric acid particles remain aqueous at all humidities in the troposphere.

[5] Previous CTM studies of the non-sea-salt ammonium-sulfate system have generally omitted the hysteresis effect, assuming either the metastable or equilibrium branch to hold throughout the atmosphere, though some studies considered both possibilities as limiting cases for radiative calculations [*Haywood and Boucher*, 2000; *Jacobson*, 2001; *Martin et al.*, 2004]. In a hybrid approach to address the hysteresis effect, *Colberg et al.* [2003] diagnosed the distribution of sulfate phase in an Eulerian CTM [*Adams et al.*, 1999] according to RH back trajectories and the monthly mean degree of neutralization ($X = [NH_4^+]/2[SO_4^{2-}]$) for each grid box.

[6] In this study, we implement a prognostic approach in a Eulerian CTM (GEOS-Chem) to simulate the hysteresis of non-sea-salt sulfate-ammonium phase transitions. Solid and aqueous particles are allowed to evolve in time as separate transported species (tracers), including conversion from one type to the other by deliquescence or crystallization. The approach tracks the solid and aqueous species in the Eulerian framework and allows solid and aqueous particles to coexist at a given location. Here we describe the model and discuss the simulated global distribution of solid and aqueous sulfate particles. A companion paper by *Wang et al.* [2008] uses the model to assess the implications for sulfate direct climate forcing.

2. Methodology

2.1. General Model Description

[7] We use the GEOS-Chem chemical transport model (version 7.03) to conduct a full year simulation of sulfate-ammonium particles [*Martin et al.*, 2004; *Park et al.*, 2004] (http://www.as-harvard.edu/chemistry/trop/geos). The simulation is driven by assimilated meteorological fields for 2001 from the NASA Goddard Earth Observing System (GEOS-3) including wind velocities, convective mass fluxes, mixing depths, clouds, temperature, humidity, precipitation, and surface properties. The GEOS-3 horizontal resolution is $1^\circ \times 1^\circ$, with 48 layers in the vertical. The temporal resolution is 6 h for the 3-D meteorological variables and 3 h for mixing depth and surface properties. The horizontal resolution is degraded here to 4° latitude by 5° longitude for input to GEOS-Chem. Advective and convective mass transport in GEOS-Chem [*Allen et al.*, 1996; *Bey et al.*, 2001] are implemented over 30-min time steps following the same schemes used in the GEOS-3 meteorological model [*Moorthi and Suarez*, 1992; *Lin and Rood*, 1996]. The mixed layer, as diagnosed by the GEOS-3 mixing depth, is homogenized every 30 min. The GEOS-3 cloud fraction data show no bias with satellite observations, indicating the reliability of the GEOS-3 meteorological data for describing large-scale dynamics and distribution of relative humidity, both of which are key factors for the simulation of particle phase transitions [*Liu et al.*, 2006].

[8] The sulfur and ammonia emissions and chemistry are as described by *Park et al.* [2004] with minor changes. Emissions are intended to be representative of the late 1990s. The global ammonia emission (including climatological biomass burning) is 55 Tg N a^{-1} [*Park et al.*, 2004]. The global anthropogenic and natural sulfur emission is 89 Tg S a^{-1}, which is 12% larger than in the work by *Park et al.* [2004], because of updated emissions in China and India [*Streets et al.*, 2003] as well as the addition of ship emissions [*Corbett et al.*, 1999]. Volcanic SO_2 emissions are from a 1990 chronology [*Andres and Kasgnoc*, 1998], including 0.7 Tg S a^{-1} eruptive and 4.8 Tg S a^{-1} noneruptive. Eruptive emissions are distributed over the appropriate months, with plume heights determined from the Volcanic Explosivity Index [*Spiro et al.*, 1992]. Noneruptive emissions are distributed evenly over the year and are released at the altitude of the volcano. The sulfate aerosols are partly or totally neutralized by ammonia (NH_3). If excess ammonia is available after the neutralization of sulfate, ammonium nitrate can be formed [*Park et al.*, 2004]. The activation of sulfate aerosols as cloud condensation nuclei is not taken into account in GEOS-Chem [*Park et al.*, 2004], but processes such as the in-cloud oxidation of sulfur into sulfate and as the deposition of sulfate aerosols through dry and wet deposition are considered. A good agreement with no bias was found for comparison of the GEOS-Chem simulated distribution of sulfate-ammonium particles and their extent of neutralization with those from the ground-based observations [*Park et al.*, 2004; *Martin et al.*, 2004].

2.2. Phase Transitions

[9] The implementation of a prognostic treatment of particle phase, including the hysteresis effect, is accomplished as follows. Five additional tracers are added to the model: solid ammonium sulfate (AS), solid letovicite (LET), solid ammonium bisulfate (AHS), aqueous sulfate (AqSulf), and aqueous ammonium (AqAmm) (Figure 1). Total sulfate (i.e., AS + LET + AHS + AqSulf) is also retained as a tracer to verify mass conservation.

[10] New production of sulfate (including direct emission) is assumed to occur in the aqueous phase. Ammonia is taken up in the aqueous phase by titration with sulfate. The conversions between solid species AS, LET, and AHS and aqueous species AqSulf and AqAmm are guided at each time step by the local RH of the grid box compared to the crystallization RH (CRH) of the aqueous species and the deliquescence RH (DRH) of the solid species (Figure 1). The CRH values of the aqueous sulfate-ammonium particles

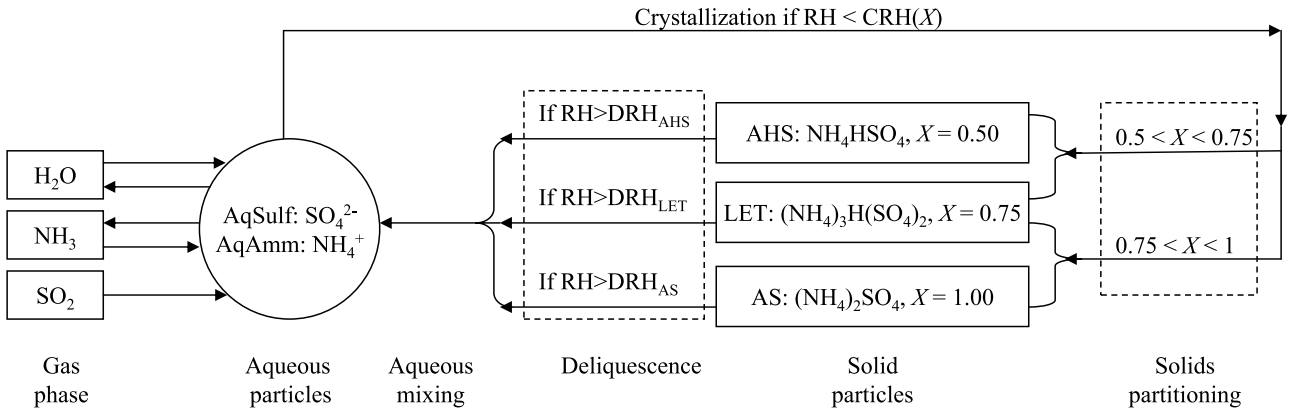

Figure 1. Schematic diagram for base case modeling in GEOS-Chem of the phase transitions of sulfate-ammonium particles. During each time step of the model, the particle phase is determined depending on the local relative humidity, the extent of neutralization, and the previous physical (phase) state. See text for details.

depend on the extent of particle neutralization ($0 \leq X \leq 1$), as follows [*Martin et al.*, 2003]:

$$X \geq 0.5: \quad CRH_0(X) = -71925 + 1690X - 139X^2 + \frac{1770760}{25 + 0.5(X - 0.7)} \tag{1a}$$

$$X < 0.5: CRH_0(X) = 0 \tag{1b}$$

The DRH_0 values for AHS, LET, and AS are 42%, 69%, and 80%, respectively [*Martin*, 2000]. Therefore, CRH_0 is defined by a continuous variable X whereas DRH_0 is defined only for $X \in \{0.5, 0.75, 1\}$. The subscript 0 indicates the reference CRH and DRH values employed in the base case and distinguishes them from those used in the sensitivity cases described in section 2.3. When crystallization of aqueous mass occurs for $0.75 < X < 1$, AS ($X = 1$) and LET ($X = 0.75$) form in proportions such that the total sulfate and ammonium mass are conserved (Figure 1). Similarly, for $0.5 < X < 0.75$, LET ($X = 0.75$) and AHS ($X = 0.5$) are formed in the correct proportions. When deliquescence occurs, AqSulf and AqAmm are updated according to the mass and the stoichiometry of the solids. By this approach, the difference between the initial and final deliquescence RH of mixed composition particles is omitted. The dependence of DRH and CRH on temperature is neglected.

[11] The upshot of this implementation is that the hysteresis effect is explicitly described. At a given model time step, no new solids form if the ambient RH exceeds CRH(X). Aqueous mass is converted to solids if the RH is less than CRH(X). Solid mass remains unchanged if the RH is less than the DRH of all three solids. If the RH exceeds the DRH of one or more of the solids, however, the mass of those solids is converted to aqueous mass. If the RH falls between the CRH and the DRH of at least one of solids, both aqueous and solid particles can coexist. The mass and charge balance of sulfate and ammonium are conserved in this implementation.

[12] The approach can be further clarified by an example. The initialization of the scenario consists of externally mixed particles of LET and AS in grid position 1 and AqSulf particles of $X = 0.9$ alone in position 2. The aerosols from these two grid positions move by advection to position 3. Phase transitions there of these different species depend on the local RH, which for this example is 60%. In this case, no phase transitions occur because the DRH values of LET and AS are 69% and 80%, respectively, and the CRH($X = 0.9$) of AqSulf is 32%. At this point, the LET and AS masses coexist with the AqSulf mass, which are all separate tracers. The separate masses then advect to grid position 4, where the local RH is 30%. The AqSulf mass crystallizes to solids, thereby incrementing the LET and AS masses in a molar sulfate ratio of 1.5:3 to hold the overall composition of $X = 0.9$. In the end, grid position 4 thus holds no AqSulf mass but does hold LET and AS masses in the amount of the increment plus the masses advected from position 3.

[13] One additional change to the standard GEOS-Chem is required because our general approach assumes constancy of RH in a grid box over the 6-h temporal resolution of the GEOS archive. This assumption is not accurate in the mixed layer at the Earth's surface for two reasons. (1) The local RH varies greatly over the die cycle of mixed layer growth and decay. (2) Fast turbulent homogenization within the mixed layer exposes particles to correspondingly fast variations in RH, from low values at the bottom near the warm surface (RH_{min}) to high values near the cold top (RH_{max}). To address this problem, we use the 3-h mixing depth information from the GEOS-3 meteorological archive, together with the 6-h temperature and specific humidity information in the lowest model layer (centered at about 10 m above the local surface). We generate RH vertical profiles within the mixed layer by assuming an adiabatic lapse rate and constancy of water vapor mixing ratio. When phase is diagnosed at each time step (30 min), we assume that air throughout the mixed layer is exposed during the time step to the range [RH_{min}, RH_{max}], with 50% of the air in a given mixed layer grid box last exposed to RH_{min} (upward motion) and 50% last exposed to RH_{max} (downward motion). These RH_{min} and RH_{max} values, combined with the local RH of the grid box, define the RH history of the aerosol particles in the mixed layer.

Table 1. Annually Averaged Species Partitioning Among Solid and Aqueous Sulfate Phases on a Sulfate Mass Basis[a]

	DRH(X) = CRH$_0$(X) "Upper Side"	Base Case	CRH(X) = DRH*(X) "Lower Side"	No Volcanic Eruption
Entire troposphere				
AS	15%	31%	48%	32%
LET	2%	3%	6%	3%
AHS	<1%	<1%	2%	<1%
AqSulf	83%	66%	44%	65%
Boundary layer[b]				
AS	11%	20%	41%	20%
LET	2%	2%	5%	2%
AHS	<1%	<1%	<1%	<1%
AqSulf	88%	77%	53%	77%
Middle troposphere[c]				
AS	14%	31%	50%	33%
LET	2%	3%	6%	3%
AHS	0%	<1%	2%	<1%
AqSulf	84%	65%	42%	63%
Upper troposphere[d]				
AS	24%	54%	55%	60%
LET	5%	5%	7%	5%
AHS	0%	<1%	2%	1%
AqSulf	71%	40%	36%	34%

[a]Results are shown for the base case accounting for full hysteresis and for upper side and lower side cases defined by DRH = CRH$_0$ and CRH = DRH*, respectively (see section 2.3). The last column shows the results for a simulation similar to the base case but without eruptive emissions from volcanoes. AS, LET, AHS, and AqSulf denote ammonium sulfate, letovicite, ammonium bisulfate, and aqueous sulfate, respectively.

[b]As determined from the mixing depths of GEOS-3 (global annual average of 884 hPa).

[c]Extending from the top of the mixed layer to 500 hPa.

[d]Extending from 500 hPa to the local tropopause of GEOS-3.

2.3. Cases Studied

[14] We conduct a full-year base simulation as described above with a 6-month spin-up to achieve initialization. Several types of sensitivity studies are also performed. The first two omits hysteresis by assuming that DRH(X) = CRH$_0$(X) or alternatively that CRH(X) = DRH*(X). These two alternatives approximately represent the lower and upper sides of the hysteresis loop, respectively. For the first study, the DRH values for AHS, LET, and AS are 0%, 24%, and 34%. For the second study, we require an artificial function DRH*(X) as a continuous function in X, rather than the discrete function DRH$_0$ ($X \in \{0.5, 0.75, 1\}$), and we use the formulation of *Schlenker and Martin* [2005]:

$$X \geq 0.75 : DRH^*(X) = -91.6X^2 + 189.57X - 18.05 \quad (2a)$$

$$0.5 \leq X < 0.75 : DRH^*(X) = -379.37X^2 + 549.11X - 127.49 \quad (2b)$$

DRH*(X) and DRH$_0$(X) are approximately equal for $X \in \{0.5, 0.75, 1\}$. No DRH*(X) is required for $X < 0.5$ because crystallization does not occur (equation (1b)).

[15] A third type of sensitivity study explores impurities that inhibit crystallization and heterogeneous nuclei that promote crystallization by running the model with positive and negative offsets to CRH$_0$(X). A final sensitivity study investigates the timescale of phase transitions by initializing the troposphere with all aqueous or all solid particles and monitoring the length of time until the model converges to steady state values of the solids mass fraction.

3. Results

3.1. Global Burdens and Neutralization of Sulfate

[16] The simulated global annul burden of sulfate is 0.33 Tg S, which is distributed as 30% in boundary layer,

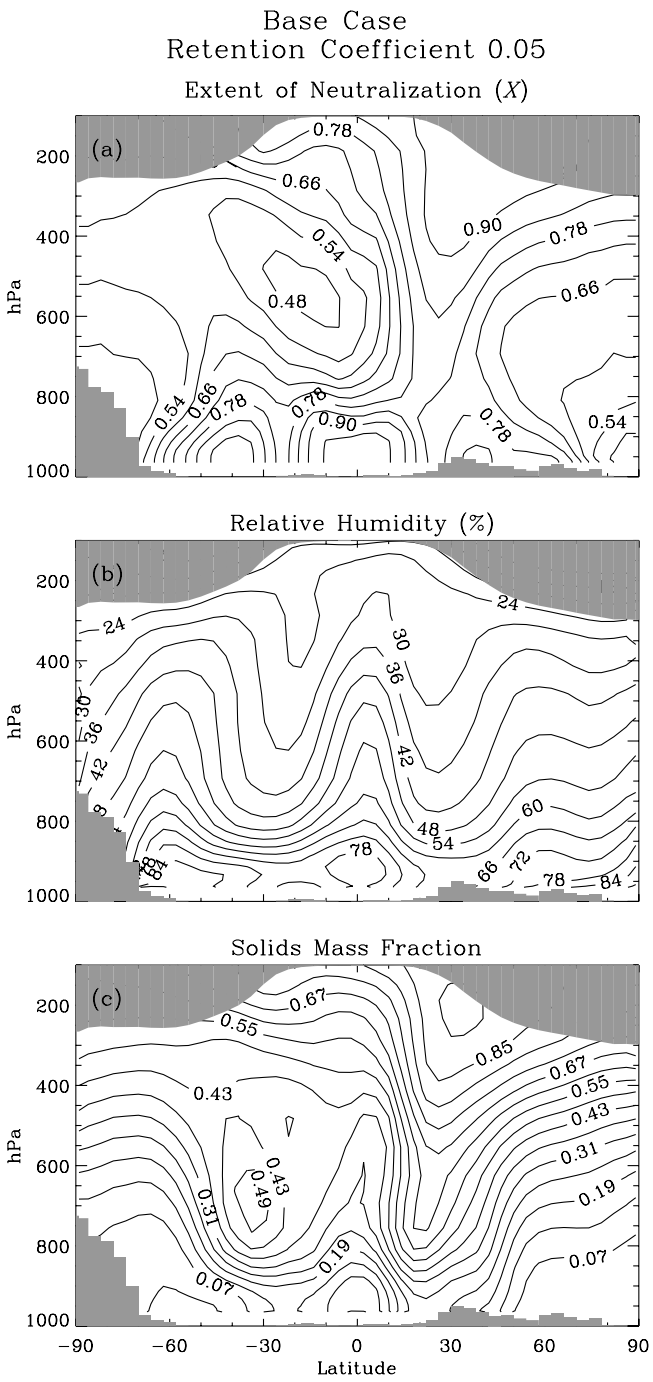

Figure 2. Annual base case zonal means of (a) the extent of neutralization X, (b) the relative humidity, and (c) the solids mass fraction using an NH_3 retention coefficient of 0.05 (see main text).

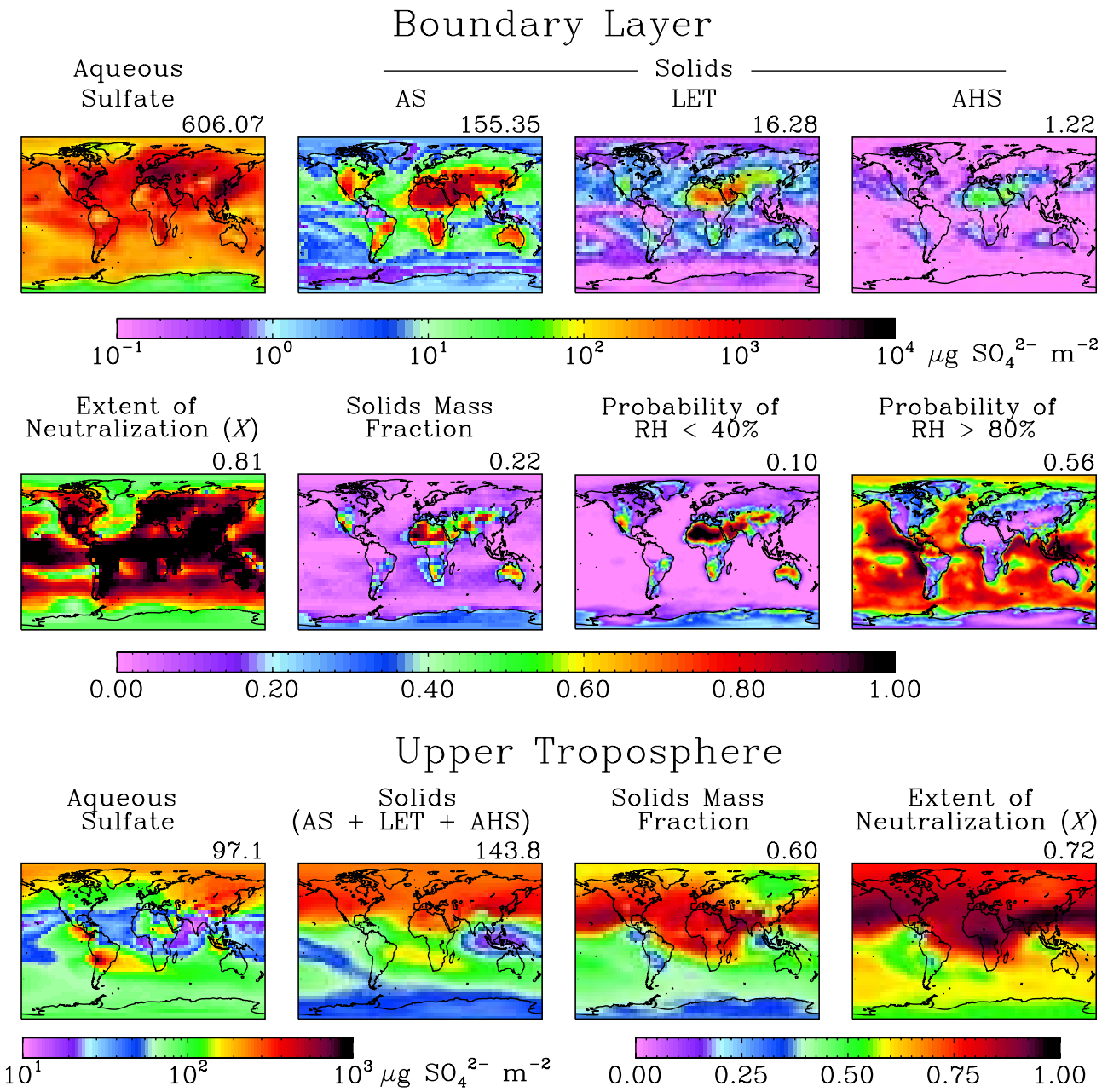

Figure 3. Geographic distribution of annually averaged quantities. (top) Boundary layer mass burden of sulfate partitioned as aqueous sulfate, solid ammonium sulfate (AS), solid letovicite (LET), and solid ammonium bisulfate (AHS). (middle) Extent of neutralization (X), solids mass fraction on a sulfate basis, percent frequency of RH < 40%, and percent frequency of RH > 80% in the boundary layer. (bottom) Upper troposphere mass burdens of solid and aqueous sulfate particles, the extent of neutralization (X), and the solids mass fraction. Upper troposphere is taken from 500 hPa to the tropopause. The number on the top right of each panel shows the corresponding globally averaged quantity.

58% in middle troposphere (up to 500 hPa), and 12% in upper troposphere. The corresponding percentages for ammonium (0.28 Tg N) are 36%, 54%, and 10%, respectively. Table 1 presents the modeled percentages of the different sulfate forms. Solid sulfate constitutes 34% of the total sulfate burden in the base case, increasing from 22% in the boundary layer to 34% in the middle troposphere to 60% in the upper troposphere. For comparison, *Colberg et al.* [2003] reported values of 18%, 28%, and 46%, respectively, for these elevations. In our simulation, 91% of solid sulfate is in the form of ammonium sulfate (Table 1), while *Colberg et al.* [2003] found that letovicite was dominant. The difference can be explained by the extent of neutralization (X) in the two simulations. *Colberg et al.* [2003] used monthly mean X data from *Adams et al.* [1999], which were generally less than 0.75 in the continental boundary layer and decreased with altitude to 0.4 in the upper troposphere. In our study, the X values are generally greater than 0.8 in the continental boundary layer and greater than 0.6 in the upper troposphere (Figures 2 and 3).

[17] The difference in X values between our study and *Adams et al.* [1999] reflects differences in both emissions and the treatment of NH_3 scavenging. *Adams et al.* [1999] specified sulfur and ammonia emissions from the Global Emissions Inventory Activity (GEIA) for 1990 [*Benkovitz et al.*, 1996; *Bouwman et al.*, 1997]. Our total ammonia emissions are the same as those of *Adams et al.* [1999], but because we account for temperature dependence our emissions are more concentrated in summer when sulfate production is also highest, thus promoting ammonium sulfate formation. *Adams et al.* [2001] pointed out that the seasonal variation of ammonia emission used by *Adams et al.* [1999] had insufficient seasonal amplitude, resulting in smaller sulfate neutralization on an annual mean basis. Our total sulfur emission is 7% larger than that used by *Adams et al.* [1999], with offsetting differences in marine dimethylsulfide (DMS) (14 Tg S a^{-1}, 36% larger) and anthropogenic (64 Tg S a^{-1}, 4% smaller) emissions. Large decreases in anthropogenic sulfur emissions in the U.S. and Europe over the past 20 years have increased the level of neutralization in the continental boundary layer, as is apparent from long-term wet deposition data [*Lehmann et al.*, 2007].

[18] Another major difference between our simulation and *Adams et al.* [1999], affecting particularly the neutralization in the upper troposphere, is our exclusion of NH_3 gas during the freezing of water droplets to ice crystals, thus allowing NH_3 to escape scavenging in deep clouds. Laboratory data indicate an NH_3 retention efficiency between 0.0001 and 0.01 upon the freezing of liquid water depending on the concentration of ammonium [*Jaccard and Levi*, 1961; *Pruppacher and Klett*, 2003]. Our simulation assumes a retention efficiency of 0.05 [*Mari et al.*, 2000], whereas most global CTMs including *Adams et al.* [1999] assume a retention efficiency of unity. A change of the retention efficiency from 0.05 to unity decreases the upper tropospheric annual mean X values by 0.3 (Figure 4a) or 40%.

[19] A high extent of neutralization for sulfate particles in the upper troposphere, with $X > 0.5$ almost everywhere (Figure 2), is consistent with the few available aircraft observations. Full sulfate neutralization was found in 70% of the air samples collected above 6 km over the South Pacific (0–30°S, 165°E–105°W) during two field campaigns [*Schultz et al.*, 2000; *Dibb et al.*, 2002]. High X values were also observed over the northern Pacific (15–40°N, 120°E–60°W) where 60% of samples above 6 km had $X > 0.5$ and 15% had $X > 0.9$ [*Dibb et al.*, 2003]. Measurements over the North Atlantic (20–70°N, 120°W–20°E) in the fall also found full neutralization in over 35% of the samples above 8 km [*Dibb et al.*, 2000]. Over the central continental U.S. in late spring, *Talbot et al.* [1998] measured an average X of 0.65 in the upper troposphere.

3.2. Global Distribution of Aqueous and Solid Particles

[20] The zonal means of the extent of neutralization, relative humidity, and solids mass fraction are shown in Figure 2. The solids mass fraction generally increases with altitude, largely following the decrease in RH. The extent of neutralization exceeds 0.9 in the upper troposphere over the northern tropics, reflecting the release of ammonia from deep continental convection. The most acidic conditions ($X < 0.5$) are in the middle troposphere of the southern tropics, as explained by (1) marine convection that injects DMS into the middle troposphere where sulfate is then produced and (2) eruptive SO_2 emissions from the Lascar volcano in Chile (volcano altitude 5.6 km) and the Sabancarya volcano in Peru (5.9 km). A simulation without these volcanoes, for example, increases the zonal averaged X values by 0.06 to 0.11 in the middle troposphere over the 0–50°S region (figure not shown). In contrast, the eruptions of Northern Hemisphere volcanoes have a much smaller impact on the zonal averages of X.

[21] The geographic distribution of mass burdens is shown in Figure 3 for the boundary layer and the upper troposphere. The mass burdens of solid particles in the boundary layer are most correlated with RH, rather than neutralization, because X is usually close to unity. There are exceptions over some oceanic and polar regions. Compared to the boundary layer, the sulfate mass burden in the upper troposphere is about one order of magnitude lower, but the solids mass burden is similar because of the higher solids mass fraction. In both hemispheres, the sulfate mass burdens in the upper troposphere are largest over the midlatitudes, reflecting the distribution of sulfur emission (including DMS) at southern midlatitudes [*Benkovitz et al.*, 1996; *Chin and Jacob*, 1996]. The solids mass fractions in the upper troposphere are largest over the tropics and northern midlatitudes, explained by the injection of ammonia from deep continental convection. Correlations apparent in Figure 3 suggest that the degree of neutralization, rather than the relative humidity, explains the distribution of the solids mass fraction in the upper troposphere, in contrast to the boundary layer where the opposite is found.

[22] Volcanic emission also affects the distribution of sulfate acidity in the upper troposphere. The total of eruptive and noneruptive volcanic sulfur emission for 1990 is 5.5 Tg S a^{-1}, lower than the mean value 7.8 Tg S a^{-1} for 1964–1972 [*Spiro et al.*, 1992]. There were in total seven eruptions in 1990 with a volcano eruptive index (VEI) of 3 (Figure 4b), producing in the model SO_2 plumes extending to 9 to 12 km and reducing the X values by 0.05–0.10 in the upper troposphere over volcano sources and nearby downwind regions (Figure 4b).

[23] The monthly variation of the solids mass fraction over both hemispheres generally follows that of X, with larger values from May to October (Figure 5). In turn, the variation of X follows the NH_3 emission, which is regulated by warmer temperatures over the Northern Hemisphere in the summer and greater biomass burning over the Southern Hemisphere at the same time. (The effect of seasonal biomass burning can be geographically identified in Figures S1 and S2[1].) The minimum in the emission of DMS in the winter of the Southern Hemisphere also contributes to the maximum of X during that period. The extent of neutralization in the upper troposphere of the Southern Hemisphere drops to nearly zero in March–April, corresponding to the large eruption from the Lascar volcano in Chile in 1990. The simulation without eruptive volcanic emissions still shows this minimum of X, though not as low (namely, 0.2).

[1] Auxiliary materials are available in the HTML. doi:10.1029/2007JD009367.

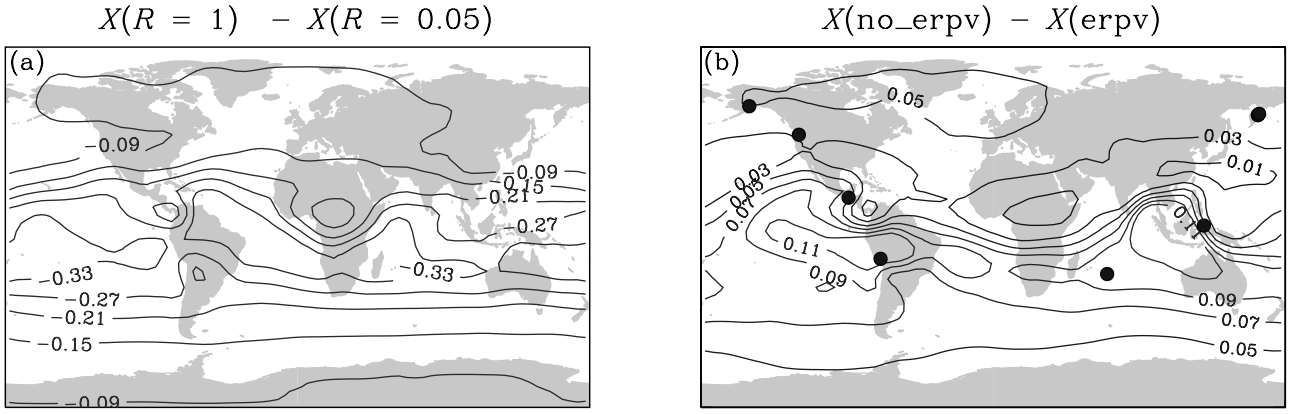

Figure 4. Difference in the extent of particle neutralization (X) in the upper troposphere for a sensitivity case compared to that of the base case. (a) Effect of the NH_3 retention efficiency (R). (b) Effect of the omission of sulfur emission from eruptive volcanoes (denoted as "no_erpv"). The dots in Figure 4b show the locations of volcanoes that had a volcano explosive index (VEI) greater than 3 in 1990 and thus had SO_2 plume heights of up to 9 km.

3.3. Omission of the Hysteresis Effect

[24] Compared to the base case, a simulation that omits hysteresis by assuming the lower side of the hysteresis loop shifts the solids mass fraction by +0.22 in the boundary layer, +0.23 in the middle troposphere, and +0.04 in the upper troposphere (Table 1). In contrast, a simulation that follows the upper side of the hysteresis loop decreases the solids mass fraction by −0.11, −0.19, and −0.31 in the boundary layer, middle troposphere, and upper troposphere, respectively. The implication is that an upper side approximation is closer to the base case than a lower side approximation, for the boundary layer and the middle

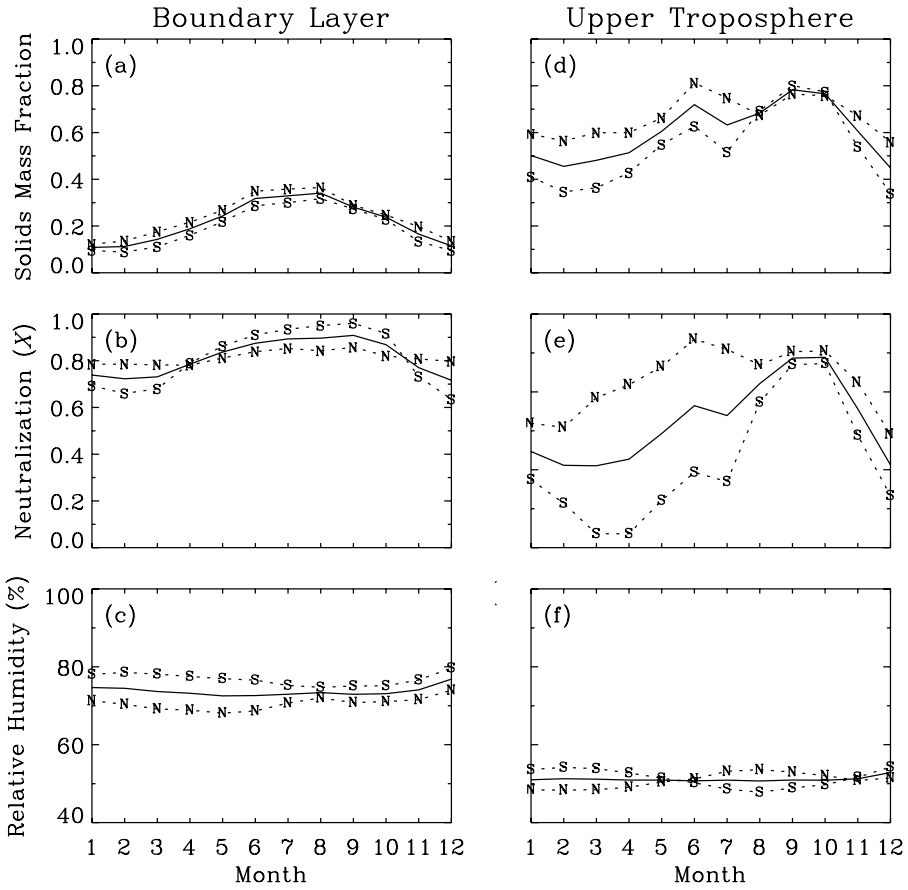

Figure 5. Seasonal variation of global averages of the solids mass fraction, the extent of neutralization (X), and the relative humidity for the boundary layer and the upper troposphere. Partitioning in the Northern ("N") and the Southern ("S") Hemispheres is also shown.

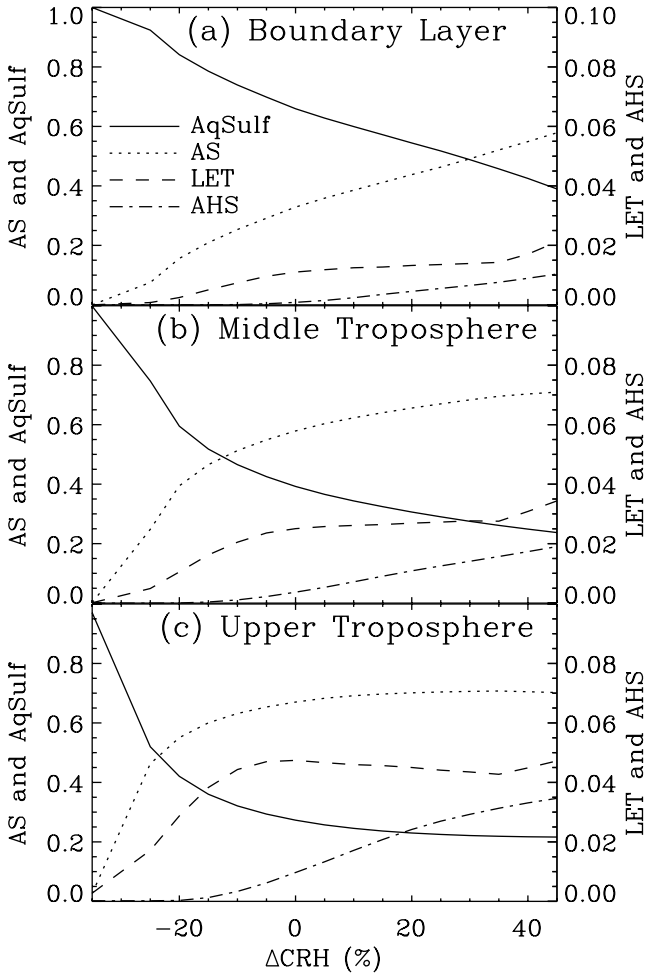

Figure 6. Sensitivity to crystallization relative humidity (CRH). Shown are the globally averaged sulfate mass fractions of aqueous sulfate (AqSulf), solid ammonium sulfate (AS), solid letovicite (LET), and solid ammonium bisulfate (AHS) for August 2001. ΔCRH(X) along the abscissa represents the perturbation to $CRH_0(X)$ of equation (1) as $CRH(X) = CRH_0(X) + \Delta CRH(X)$. Further constraints are (1) $CRH(X) = 0$ for $(CRH_0(X) + \Delta CRH(X)) < 0$ and (2) $CRH(X) = DRH^*(X)$ for $(CRH_0(X) + \Delta CRH(X)) > DRH^*(X)$ (see equation (2)).

troposphere. A lower side approximation is more accurate for the upper troposphere, where the RH falls more often below the CRH of ammonium sulfate, leading to dominance of the lower side of the hysteresis loop given the high extent of neutralization.

3.4. Effects of Composition on Hysteresis

[25] In the actual atmosphere, the phase transitions of sulfate particles are more complicated than given by the sulfate-ammonium system. The presence of organic molecules or nitrate ions tends to decrease the CRH and the DRH, while insoluble components such as mineral dust tend to increase the CRH [*Martin et al.*, 2001, 2003, 2004; *Braban and Abbatt*, 2004; *Parsons et al.*, 2004, 2006]. To address the effects of changes in CRH, we carried out a sensitivity study in which the CRH of equation (1) was progressively offset in steps of 5% (i.e., ΔCRH). The dependence of sulfate phase on ΔCRH is shown in Figure 6 for different altitude ranges. For the range of ΔCRH shown in Figure 6, AS always dominates the budget of solid sulfate, although the fractions of LET and AHS increase slightly as ΔCRH increases. In the boundary layer, the solids mass fraction responds almost linearly to ΔCRH, increasing from nearly 0.0 for $\Delta CRH = -25\%$ to 0.60 for $\Delta CRH = +40\%$. In the middle and upper troposphere, the solids mass fraction is almost insensitive to ΔCRH in the range $-20\% < \Delta CRH < 40\%$ because of the generally dry conditions. Our prediction of a large solids mass fraction in the upper troposphere thus appears robust, at least in the absence of exceptional volcanic activity. Photochemical model studies of the NO_x budget in the tropical upper troposphere have previously speculated that the particles there had to be mostly solid to prevent N_2O_5 hydrolysis from being a major NO_x sink [*McKeen et al.*, 1997; *Schultz et al.*, 2000]. Since solid ammonium sulfate particles in the upper troposphere could serve as heterogeneous ice nuclei [*Shilling et al.*, 2006], our results also have important implications for cirrus cloud formation and properties [*Martin*, 1998; *Abbatt et al.*, 2006].

[26] We also investigated how decreases in the DRH values affect the solids mass fraction. In the limit of $DRH(X) = CRH_0(X)$ (e.g., $\Delta DRH = -45\%$ for AS), the solids mass fraction decreases to 17% for the whole troposphere, compared to 34% for the base case, although it remains as high as 30% in the upper troposphere (Table 1). In another sensitivity test in which the DRH values of AS, LET, and AHS were each decreased by 10% (i.e., $\Delta DRH = -10\%$), the solids mass fractions in the upper, middle, and lower troposphere dropped to 54%, 31%, and 21%, respectively, compared to 60%, 35%, and 23% in the base case.

3.5. Timescales for Phase Transitions in the Troposphere

[27] An estimate for the typical timescales of particle phase transitions in the troposphere is useful for applications such as Lagrangian back trajectory interpretation of field observations. We investigated these timescales by initializing atmospheric sulfate as either all solid or all aqueous, and observing the time required for the solid and aqueous sulfate mass fractions to return to their steady state values (Figure 7). Two timescales are apparent in Figure 7, one that is instantaneous at the beginning of the plots and a second that is 10–50 h in the boundary layer and 150–400 h in the upper troposphere.

[28] For the world in an initial state of aqueous particles, in both the boundary layer and the upper troposphere, much of the mass crystallizes instantaneously in the first time step so that AqSulf does not begin at 100% in the plot. Likewise, for the world in an initial state of solid particles, much of the mass deliquesces in the first time step so that AqSulf does not begin at 0% in the plot, though just for the boundary layer. In the upper troposphere, AqSulf does begin at 0%. The instantaneous response occurs when the local RH at time zero converts a portion of the mass from one phase to another. In the continental mixed layer, a second effect is that the $[RH_{min}, RH_{max}]$ range often extends beyond the local CRH and DRH values, in which case the loss of initial conditions is instantaneous.

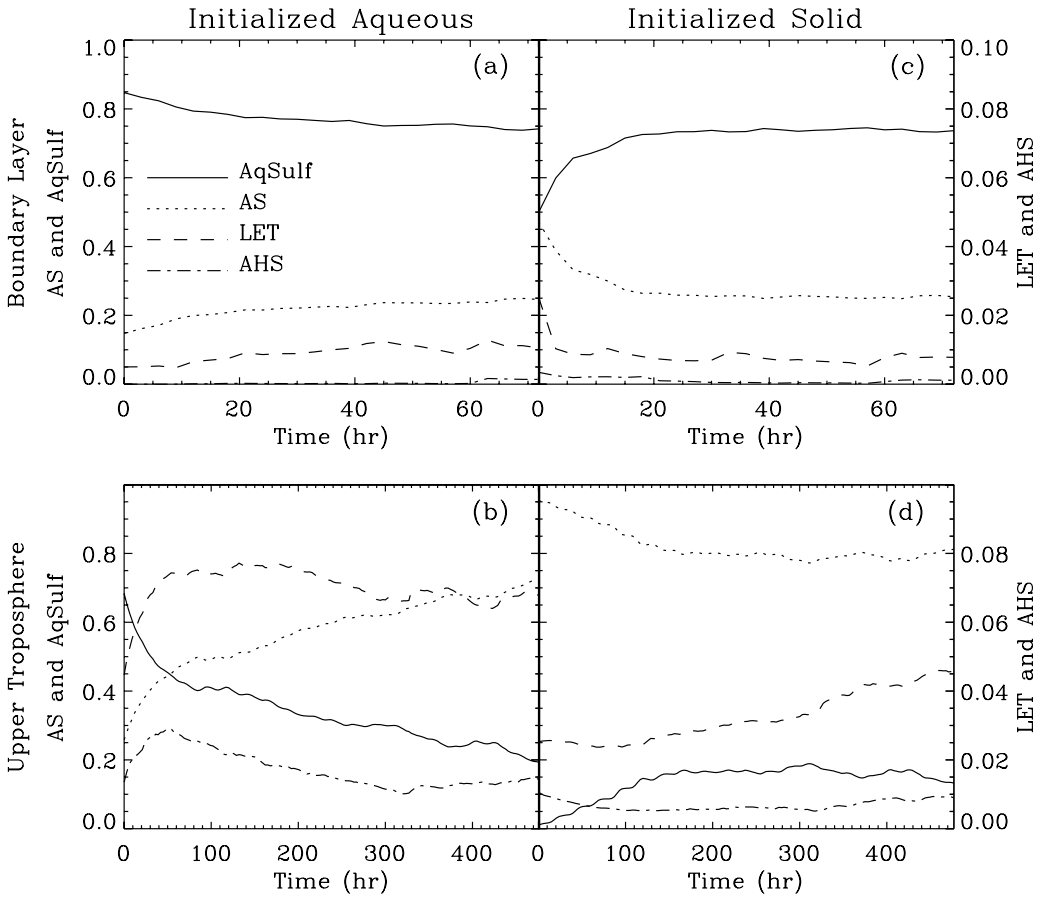

Figure 7. Temporal evolution of sulfate mass fractions of aqueous sulfate (AqSulf), solid ammonium sulfate (AS), solid letovicite (LET), and solid ammonium bisulfate (AHS) from initial states of (left) all aqueous and (right) all solid. Results are shown for (top) the boundary layer and (bottom) the upper troposphere for August 2001. (For the world in an initial state of solids, much of the mass deliquesces in the first time step so that AqSulf does not begin at 0% in the plot. See text in section 3.5.)

[29] After the instantaneous response, the solid and aqueous sulfate mass fractions return to their steady state values, doing so more quickly in the boundary layer than in the upper troposphere. These timescales in large part reflect the variability in RH in the different regions of the atmosphere. The boundary layer has both rapid mixing and large RH vertical gradients. The variability of RH in the upper troposphere is much less, and the RH often lies in metastable regions of CRH < RH < DRH.

4. Conclusions

[30] A simulation of the solid-aqueous phase transitions of non-sea-salt sulfate-ammonium particles has been implemented in the GEOS-Chem global 3-D chemical transport model. The simulation explicitly includes consideration of the metastable behavior of aqueous sulfate particles in the CRH < RH < DRH range. Though with the minor simplification that the initial and final deliquescence RH of mixed composition particles are equal, the hysteresis effect is treated by transporting aqueous and three solid sulfate phases in the CTM to retain the impact of RH history on sulfate phase and then diagnosing the phase changes every 30 min on the basis of local relative humidity.

[31] We find that the solids mass fraction on a sulfate basis is 0.34. Ammonium sulfate constitutes 93% of the solid sulfate mass, with the balance from letovicite (6%) and ammonium bisulfate (1%). A previous CTM simulation by *Colberg et al.* [2003] found a solids mass fraction 5–10% smaller than ours and dominated by letovicite. The extent of neutralization is greater in our simulation because of differences in emission inventories and ammonia scavenging. We account for the release of ammonia scavenged by cloud droplets upon droplet freezing, using a retention efficiency of 0.05. Deep convection then injects ammonia into the upper troposphere. We thus find that sulfate particles in the upper troposphere are widely neutralized, consistent with the few available observations. This has important implications for atmospheric chemistry, specifically N_2O_5 hydrolysis [*McKeen et al.*, 1997], and also for cirrus cloud nucleation [*Martin*, 1998; *Abbatt et al.*, 2006].

[32] The solids mass fraction generally increases with altitude, ranging from 22% in the boundary layer to 34% in middle troposphere to 60% in the upper troposphere. The timescale of phase transitions as driven by changes in RH varies from 10 to 50 h in the boundary layer to 150–400 h in the upper troposphere. The geographic distribution of solids in the boundary layer is regulated more by the variation in

RH than by particle neutralization. The opposite is the case in the upper troposphere.

[33] The solids mass fraction peaks from May to October in both hemispheres, largely reflecting emissions. The principal factor in the Northern Hemisphere is the summertime maximum in NH_3 biogenic emission. In the Southern Hemisphere, the principal factors are the winter minimum in DMS emission and the springtime maximum in NH_3 emission form biomass burning. Conversely, volcanic eruptions can lead to high acidity in the upper troposphere, as seen in our simulation year for a Chilean volcano in March–April.

[34] Omission of the hysteresis effect in global models by assuming that particle phase follows the lower side of the hysteresis loop increases the solids mass fraction from 0.34 to 0.56. An upper side assumption decreases the fraction to 0.17. Lower and upper side assumptions better approximate particle phase for high and low altitudes, respectively.

[35] The CRH of metastable sulfate particles is sensitive to other particle components besides ammonia, and we evaluated how shifting the CRH down (due to internal mixing with species such as organic molecules or nitrate) or up (due to mixing with heterogeneous nuclei such as mineral dust) affects phase partitioning. The solids mass fraction is highly sensitive to ΔCRH in the boundary layer but is almost independent of ΔCRH in the upper troposphere for the range $-20\% < \Delta\text{CRH} < +40\%$. Our finding of a large percentage of sulfate solids in the upper troposphere should thus be insensitive to details in the sulfate particle composition, although the model results must yet be validated by in situ observations of sulfate phase. Our work corroborates past speculation that the upper tropospheric sulfate mostly is in the solid phase, with implications for heterogeneous chemistry and cirrus cloud nucleation [*Schultz et al.*, 2000; *Abbatt et al.*, 2006].

[36] **Acknowledgments.** This research was supported by the National Science Foundation (Martin, grant ATM-0317583) and the NASA Atmospheric Composition Modeling and Analysis Program (Jacob). J. Wang was supported by the NOAA Climate and Global Change postdoctoral fellowship program under the administration of the Visiting Scientist Program in UCAR.

References

Abbatt, J. P. D., S. Benz, D. J. Cziczo, Z. Kanji, U. Lohmann, and O. Mohler (2006), Solid ammonium sulfate aerosols as ice nuclei: A pathway for cirrus cloud formation, *Science*, *313*, 1770–1773, doi:10.1126/science.1129726.

Adams, P. J., J. H. Seinfeld, and D. M. Koch (1999), Global concentrations of tropospheric sulfate, nitrate, and ammonium aerosol simulated in a general circulation model, *J. Geophys. Res.*, *104*, 13,791–13,823, doi:10.1029/1999JD900083.

Adams, P. J., J. H. Seinfeld, D. Koch, L. Mickley, and D. Jacob (2001), General circulation model assessment of direct radiative forcing by the sulfate-nitrate-ammonium-water inorganic aerosol system, *J. Geophys. Res.*, *106*, 1097–1111, doi:10.1029/2000JD900512.

Allen, D. J., R. B. Rood, A. M. Thompson, and R. D. Hidson (1996), Three-dimension ^{222}Rn calculations using assimilated data and a convective mixing algorithm, *J. Geophys. Res.*, *101*, 6871–6881, doi:10.1029/95JD03408.

Andres, R. J., and A. D. Kasgnoc (1998), A time-averaged inventory of subaerial volcanic sulfur emissions, *J. Geophys. Res.*, *103*, 25,251–25,261, doi:10.1029/98JD02091.

Benkovitz, C. M., M. T. Scholtz, J. Pacyna, L. Tarrason, J. Dignon, E. C. Voldner, P. A. Spiro, J. A. Logan, and T. E. Graedel (1996), Global gridded inventories of anthropogenic emissions of sulfur and nitrogen, *J. Geophys. Res.*, *101*, 29,239–29,253, doi:10.1029/96JD00126.

Bey, I., D. J. Jacob, R. M. Yantosca, J. A. Logan, B. Field, A. M. Fiore, Q. Li, H. Liu, L. J. Mickley, and M. Schultz (2001), Global modeling of tropospheric chemistry with assimilated meteorology: Model description and evaluation, *J. Geophys. Res.*, *106*, 23,073–23,096, doi:10.1029/2001JD000807.

Biskos, G., A. Malinowski, L. M. Russell, P. R. Buseck, and S. T. Martin (2006a), Nanosize effect on the deliquescence and the efflorescence of sodium chloride nanoparticles, *Aerosol Sci. Technol.*, *40*, 97–106, doi:10.1080/02786820500484396.

Biskos, G., D. Paulsen, L. M. Russell, P. R. Buseck, and S. T. Martin (2006b), Prompt deliquescence and efflorescence of aerosol nanoparticles, *Atmos. Chem. Phys.*, *6*, 4633–4642.

Bouwman, A. F., D. S. Lee, W. A. H. Asman, F. J. Dentener, K. W. Van Der Hoek, and J. G. J. Olivier (1997), A global high-resolution emission inventory for ammonia, *Global Biogeochem. Cycles*, *11*, 561–587, doi:10.1029/97GB02266.

Braban, C. F., and J. P. D. Abbatt (2004), A study of the phase transition behavior of internally mixed ammonium sulfate-malonic acid aerosols, *Atmos. Chem. Phys.*, *4*, 1451–1459.

Chin, M., and D. J. Jacob (1996), Anthropogenic and natural contributions to tropospheric sulfate: A global model analysis, *J. Geophys. Res.*, *101*, 18,691–18,699, doi:10.1029/96JD01222.

Clegg, S. L., P. Brimblecombe, and A. S. Wexler (1998), Thermodynamic model of the system H^+-NH_4^+-Na^+-SO_4^{2-}–NO_3^-–Cl^-–H_2O at 298.15 K, *J. Phys. Chem. A*, *102*, 2155–2171, doi:10.1021/jp973043j.

Colberg, C. A., B. P. Luo, H. Wernli, T. Koop, and T. Peter (2003), A novel model to predict the physical state of atmospheric $H_2SO_4/NH_3/H_2O$ aerosol particles, *Atmos. Chem. Phys.*, *3*, 909–924.

Corbett, J. J., P. S. Fischbeck, and S. N. Pandis (1999), Global nitrogen and sulfur inventories for ocean-going ships, *J. Geophys. Res.*, *104*, 3457–3470, doi:10.1029/1998JD100040.

Dibb, J. E., R. W. Talbot, and E. M. Scheuer (2000), Composition and distribution of aerosols over the North Atlantic during the Subsonic Assessment Ozone and Nitrogen Oxide Experiment (SONEX), *J. Geophys. Res.*, *105*, 3709–3717, doi:10.1029/1999JD900424.

Dibb, J. E., R. W. Talbot, G. Seid, C. Jordan, E. Scheuer, E. Atlas, N. J. Blake, and D. R. Blake (2002), Airborne sampling of aerosol particles: Comparison between surface sampling at Christmas Island and P-3 sampling during PEM-Tropics B, *J. Geophys. Res.*, *107*, 8230, doi:10.1029/2001JD000408 [printed *108*(D2), 2003].

Dibb, J. E., R. W. Talbot, E. M. Scheuer, G. Seid, M. A. Avery, and H. B. Singh (2003), Aerosol chemical composition in Asian continental outflow during the TRACE-P campaign: Comparison with PEM-West B, *J. Geophys. Res.*, *108*(D21), 8815, doi:10.1029/2002JD003111.

Haywood, J., and O. Boucher (2000), Estimates of the direct and indirect radiative forcing due to tropospheric aerosols: A review, *Rev. Geophys.*, *38*, 513–543, doi:10.1029/1999RG000078.

Jaccard, C., and L. Levi (1961), Ségrégation d'impuretés dans la glace, *Z. Agewandte Math. Phys.*, *12*, 70–76, doi:10.1007/BF01601109.

Jacob, D. J. (2000), Heterogeneous chemistry and tropospheric ozone, *Atmos. Environ.*, *34*, 2131–2159, doi:10.1016/S1352-2310(99)00462-8.

Jacobson, M. Z. (2001), Global direct radiative forcing due to multicomponent anthropogenic and natural aerosols, *J. Geophys. Res.*, *106*, 1551–1568, doi:10.1029/2000JD900514.

Kane, S. M., F. Caloz, and M. T. Leu (2001), Heterogeneous uptake of gaseous N_2O_5 by $(NH_4)_2SO_4$, NH_4HSO_4, and H_2SO_4 aerosols, *J. Phys. Chem. A*, *105*, 6465–6470, doi:10.1021/jp010490x.

Lehmann, C. M. B., V. C. Bowersox, R. S. Larson, and S. M. Larson (2007), Monitoring long-term trends in sulfate and ammonium in US precipitation: Results from the National Atmospheric Deposition Program/National Trends Network, *Water Air Soil Pollut.*, *7*, 59–66, doi:10.1007/s11267-006-9100-z.

Lim, H. J., A. G. Carlton, and B. J. Turpin (2005), Isoprene forms secondary organic aerosol through cloud processing: Model simulations, *Environ. Sci. Technol.*, *39*, 4441–4446, doi:10.1021/es048039h.

Lin, S.-J., and R. B. Rood (1996), Multidimensional flux from semi-Lagrangian transport scheme, *Mon. Weather Rev.*, *124*, 2046–2070, doi:10.1175/1520-0493(1996)124<2046:MFFSLT>2.0.CO;2.

Liu, H., et al. (2006), Radiative effect of clouds on tropospheric chemistry in a global three-dimensional chemical transport model, *J. Geophys. Res.*, *111*, D20303, doi:10.1029/2005JD006403.

Mari, C., D. J. Jacob, and P. Bechtold (2000), Transport and scavenging of soluble gases in a deep convective cloud, *J. Geophys. Res.*, *105*, 22,255–22,267, doi:10.1029/2000JD900211.

Martin, S. T. (1998), Phase transformations of the ternary system $(NH_4)_2SO_4$-H_2SO_4-H_2O and the implications for cirrus cloud formation, *Geophys. Res. Lett.*, *25*, 1657–1660, doi:10.1029/98GL00634.

Martin, S. T. (2000), Phase transitions of aqueous atmospheric particles, *Chem. Rev.*, *100*, 3403–3453, doi:10.1021/cr990034t.

Martin, S. T., J. H. Han, and H. M. Hung (2001), The size effect of hematite and corundum inclusions on the efflorescence relative humidities of aqueous ammonium sulfate particles, *Geophys. Res. Lett.*, *28*, 2601–2604, doi:10.1029/2001GL013120.

Martin, S. T., J. C. Schlenker, A. Malinowski, H. M. Hung, and Y. Rudich (2003), Crystallization of atmospheric sulfate-nitrate-ammonium particles, *Geophys. Res. Lett.*, *30*(21), 2102, doi:10.1029/2003GL017930.

Martin, S. T., H. M. Hung, R. J. Park, D. J. Jacob, R. J. D. Spurr, K. V. Chance, and M. Chin (2004), Effects of the physical state of tropospheric ammonium-sulfate-nitrate particles on global aerosol direct radiative forcing, *Atmos. Chem. Phys.*, *4*, 183–214.

McKeen, S. A., T. Gierczak, J. B. Burkholder, P. O. Wennberg, T. F. Hanisco, E. R. Keim, R.-S. Gao, S. C. Liu, A. R. Ravishankara, and D. W. Fahey (1997), The photochemistry of acetone in the upper troposphere: A source of odd-hydrogen radicals, *Geophys. Res. Lett.*, *24*, 3177–3180, doi:10.1029/97GL03349.

Moorthi, S., and M. J. Suarez (1992), Relaxed Arakawa-Schubert. A parameterizaiton of moist convection for general circulation models, *Mon. Weather Rev.*, *120*, 978–1002, doi:10.1175/1520-0493(1992)120<0978:RASAPO>2.0.CO;2.

Park, R. J., D. J. Jacob, B. D. Field, R. M. Yantosca, and M. Chin (2004), Natural and transboundary pollution influences on sulfate-nitrate-ammonium aerosols in the United States: Implications for policy, *J. Geophys. Res.*, *109*, D15204, doi:10.1029/2003JD004473.

Parsons, M. T., D. A. Knopf, and A. K. Bertram (2004), Deliquescence and crystallization of ammonium sulfate particles internally mixed with water-soluble organic compounds, *J. Phys. Chem. A*, *108*, 11,600–11,608, doi:10.1021/jp0462862.

Parsons, M. T., J. L. Riffell, and A. K. Bertram (2006), Crystallization of aqueous inorganic-malonic acid particles: Nucleation rates, dependence on size, and dependence on the ammonium-to-sulfate ratio, *J. Phys. Chem. A*, *110*, 8108–8115, doi:10.1021/jp057074n.

Pruppacher, H. R., and J. D. Klett (2003), *Microphysics of Clouds and Precipitation*, pp. 163–164, Springer, New York.

Ramaswamy, V., et al. (2001), Radiative forcing of climate change, in *Climate Change 2001: The Scientific Basis—Contribution of Working Group I to the Third Assessment Report of the Intergovernmental Panel on climate Change*, edited by J. T. Houghton et al., pp. 349–416, Cambridge Univ. Press, New York.

Schlenker, J. C., and S. T. Martin (2005), Crystallization pathways of sulfate-nitrate-ammonium aerosol particles, *J. Phys. Chem. A*, *109*, 9980–9985, doi:10.1021/jp052973x.

Schultz, M. G., D. J. Jacob, J. D. Bradshaw, S. T. Sandholm, J. E. Dibb, R. W. Talbot, and H. B. Singh (2000), Chemical NO_x budget in the upper troposphere over the tropical south Pacific, *J. Geophys. Res.*, *105*, 6669–6679, doi:10.1029/1999JD900994.

Seinfeld, J. H., and S. N. Pandis (1998), *Atmospheric Chemistry and Physics*, John Wiley, New York.

Shilling, J. E., T. J. Fortin, and M. A. Tolbert (2006), Depositional ice nucleation on crystalline organic and inorganic solids, *J. Geophys. Res.*, *111*, D12204, doi:10.1029/2005JD006664.

Spann, J. F., and C. B. Richardson (1985), Measurement of the water cycle in mixed ammonium acid sulfate particles, *Atmos. Environ.*, *19*, 819–825, doi:10.1016/0004-6981(85)90072-1.

Spiro, P. A., D. J. Jacob, and J. A. Logan (1992), Global inventory of sulfur emissions with $1° \times 1°$ resolution, *J. Geophys. Res.*, *97*, 6023–6036.

Streets, D. G., et al. (2003), An inventory of gaseous and primary aerosol emissions in Asia in the year 2000, *J. Geophys. Res.*, *108*(D21), 8809, doi:10.1029/2002JD003093.

Talbot, R. W., J. E. Dibb, and M. B. Loomis (1998), Influence of vertical transport on free tropospheric aerosols over the central USA in springtime, *Geophys. Res. Lett.*, *25*, 1367–1370, doi:10.1029/98GL00184.

Tang, I. N., and H. R. Munkelwitz (1994), Aerosol phase-transformation and growth in the atmosphere, *J. Appl. Meteorol.*, *33*, 791–796, doi:10.1175/1520-0450(1994)033<0791:APTAGI>2.0.CO;2.

Wang, J., and S. T. Martin (2007), Satellite characterization of urban aerosols: Importance of including hygroscopicity and mixing state in the retrieval algorithms, *J. Geophys. Res.*, *112*, D17203, doi:10.1029/2006JD008078.

Wang, J., D. J. Jacob, and S. T. Martin (2008), Sensitivity of sulfate direct climate forcing to the hysteresis of particle phase transitions, *J. Geophys. Res.*, *113*, D11207, doi:10.1029/2007JD009368.

A. A. Hoffmann, D. J. Jacob, and S. T. Martin, School of Engineering and Applied Sciences, Harvard University, Cambridge, MA 02138, USA. (scot_martin@harvard.edu)

R. J. Park, School of Earth and Environmental Sciences, Seoul National University, San 56-1, Sillim, Gwanakgu, Seoul 151-742, South Korea.

J. Wang, Department of Geosciences, University of Nebraska–Lincoln, Lincoln, NE 68588, USA. (jwang7@unl.edu)